IEEE Access
Multidisciplinary | Rapid Review | Open Access Journal

Received January 31, 2020, accepted February 18, 2020, date of publication February 21, 2020, date of current version March 3, 2020.

Digital Object Identifier 10.1109/ACCESS.2020.2975596

Cooperative Control for Multi-Excitation Units WPT System With Multiple Coupling Parameter Identification and Area Adaptation

XIN DAI[1,2], (Member, IEEE), JINCHENG JIANG[1], ZHOU XU[3], AND YANLING LI[4]

[1]School of Automation, Chongqing University, Chongqing 400044, China
[2]National Center of International Research on Wireless Power Transfer Technology, Chongqing 400044, China
[3]China Mobile IoT Company, Chongqing 400044, China
[4]School of Electrical Engineering and Electronics Information, Xihua University, Chengdu 610039, China

Corresponding author: Xin Dai (toybear@vip.sina.com)

This work was supported by the National Natural Science Foundation of China under Grant 51777022.

ABSTRACT In a multiple excitation unit wireless power transfer system, power control flexibility is a critical feature. To develop a system with environmental sensing capability and a smart power distribution strategy, a cooperative control method is proposed for the excitation units. A multiple coupling coefficient identification method was developed by utilizing the DC information of each excitation unit. Furthermore, a bi-operation mode with adaptive area division is proposed to achieve maximum efficiency in the optimum coupling area and to satisfy the fundamental power requirement for a weak coupling area. In the identification and control implementation process, this method is easy to implement and the response speed can be guaranteed because only the DC input current and the duty cycle of the DC regulator information are required. In addition, the proposed approach was evaluated based on experimental analysis.

INDEX TERMS Coupling parameter, maximum efficiency, multi-excitation units, observation Wireless power system.

I. INTRODUCTION

Multiple excitation unit wireless power transfer system (MEU-WPT) technology integrates energy from several excitation transmitters to provide a receiver with a relatively large power output. Compared with a classical single excitation unit system, the MEU system has more flexible power control, is more tolerant with respect to loads and coupling variation, and exerts less stress on the switching components. Therefore, MEU technology has been increasingly utilized in a range of applications in recent years such as drone charging, power supply of multiple mobile electronic devices, and electric vehicle charging [1]–[5]. The main advantages of this method include: 1) large power transfer capacity; 2) high misalignment tolerance; 3) flexible power output; 4) high system efficiency (under some condition [15]); 5) low voltage and current stress on a single excitation unit [6]–[9].

As one of the notable features of MEU-WPT systems, the flexibility of power control has been a significant research area in the recent two years. In a published paper [10], a control criterion was presented for a multi-transmitter system, and the corresponding switch group structure was constructed to realize switching control. The control criteria were applied to select the optimal working mode under coil lateral misalignment. In a published paper [11], to solve the resonant frequency shifting issue caused by a load change, an automatic frequency tracking method was developed to ensure that the maximum possible energy transfer efficiency for any number of loadings. In addition, a multi-loading decoupling control mechanism was also demonstrated, whereby each secondary coil received a consistent supply of energy without being affected by the addition or removal of a coil. Paper [12] investigated an analytical solution for the theoretical optimum transmitter current using a current-amplitude modulation scheme based on the analogy of the N-dimensional Cartesian coordinate equivalent of spherical coordinates to achieve the maximum efficiency of the system. Paper [13] presented a simple abstract approach for modeling a WPT system using multiple transmitter coils that attempt to transfer power to a single receiver coil. The optimal excitation current

The associate editor coordinating the review of this manuscript and approving it for publication was Mohamed Kheir.

vector was obtained to achieve maximum efficiency. In paper [14], several parallel reactive power compensation networks (RPCNs) were adopted to form an energy transmitting pad array on the primary side. These RPCNs were excited by a single primary converter. A current regulation circuit and corresponding control method were proposed to regulate the primary current in every primary coil in the pad array to reduce the EMI and improve system's efficiency. In paper [15], a PWM control method is proposed to keep the resonant current in phase so as to achieve the output optimization by detecting the phase difference of AC current in resonant tank. However, AC detection has some delay and low accuracy, which increases the complexity of the system circuit.

Although output power control of MEU-WPT systems have been investigated in several studies, there still exist many challenges with respect to application such as: 1) multiple coupling coefficient identification is an inevitable issue in a WPT system with multiple excitation units; 2) multiple coupling among excitation units and pickups will have a great influence on power distribution strategy. However, due to its complexity, solutions have not been advanced. 3) Considering the excitation unit matrix, there exists an optimum and weak optimal power transfer area. The energy distribution strategy must be adjusted to achieve the best performance according to the dynamics of the area division.

Most importantly, with batch production and cost reduction of single WPT units, it is relatively easy to construct a WPT area with numerous excitation units. Therefore, cooperative control will play an increasingly important role in MEU-WPT systems in terms of providing a more flexible and convenient user experience for WPT products.

With the objective of developing a MEU-WPT system with environmental sensing capability and smart power distribution strategy, a cooperative control method for MEU-WPT systems is proposed in this paper. Multiple coupling coefficient identification methods are presented by using the input DC information of each excitation unit. On this basis, an adaptive coupling area division method is outlined to divide the matrix excitation area into optimum and weak coupling areas. To meet the high-efficiency requirements in the optimum coupling area in addition to the fundamental output power requirements in the weak coupling area, a cooperative control strategy is proposed to achieve the best performance using an adaptive approach. In the identification and control flow, this method is easy to implement and the response speed can be guaranteed because only the DC input current and the duty cycle of the DC regulator information are required.

II. DESIGN OF THE PROPOSED MEU-WPT SYSTEM

Compared with a traditional single excitation system, the MEU-WPT system has a relatively complex coupling area at the primary side. Therefore, it is necessary to select an optimum system operation mode to achieve optimum performance [5], [16]–[21]. In this section, an area automatic division method will be presented according to the optimal

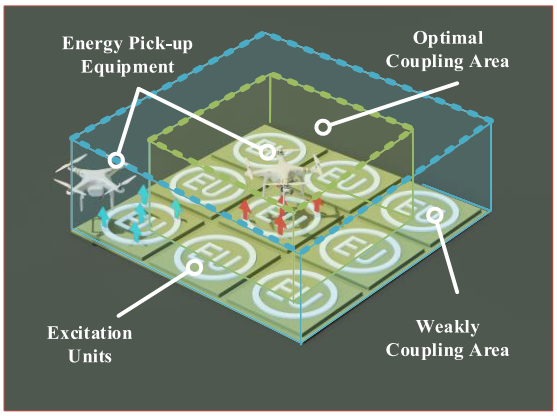

FIGURE 1. Multi-excitation unit wireless power system.

coupling area and weakly coupling conditions. Moreover, different control modes will be proposed for different area.

Fig. 1 shows the coupling area of the MEU-WPT system. This area can be divided into the optimum coupling area and the weakly coupling area. In the former, the system's efficiency is the most important factor. In the latter, the satisfaction of the fundamental power requirements of the load will be considered. However, it should be noted that the area division is not fixed and will dynamically change according to the load power requirements.

Fig. 2 displays the topology of the MEU-WPT system. There are 3 excitation units at the primary side and single pickup at the secondary side. DC-DC regulators are placed in front of each excitation unit to control the input power, where $L_{p1}, L_{p2} \ldots L_{pn}$ are the primary inductors and L_s is the secondary inductor. $C_{p1}, C_{p2} \ldots C_{pn}$ and C_s are the resonant capacitors and $i_{p1}, i_{p2} \ldots i_{pn}$ are the resonant current. The parameters $u_1, u_2 \ldots u_n$ are the output voltage of the inverter and $I_{in1}, I_{in2} \ldots I_{inn}$ are the direct currents of the system. $Z_{r1}, Z_{r2} \ldots Z_{rn}$ are the equivalent impedance of the resonant network, C_o is the filter capacitor of the rectifier circuit, and R_L is the equivalent load resistance. M_i is the mutual inductance between the primary coil and secondary and coil M_{ij} is the cross-coupling.

According to KVL's law, the relationship between the currents and voltages can be derived as equation (1) as follows:

$$\begin{bmatrix} \dot{u}_1 \\ \dot{u}_2 \\ \vdots \\ \dot{u}_n \\ 0 \end{bmatrix} = \begin{bmatrix} R_{p1} & j\omega \mathrm{M}_{12} & \cdots & j\omega M_{1n} & j\omega M_1 \\ j\omega M_{21} & R_{p2} & \cdots & j\omega M_{2n} & j\omega M_2 \\ \vdots & \vdots & \vdots & \vdots & \vdots \\ j\omega M_{n1} & j\omega M_{n2} & \cdots & R_{pn} & j\omega M_n \\ j\omega M_1 & j\omega M_2 & \cdots & j\omega M_n & R_o + R_s \end{bmatrix} \begin{bmatrix} \dot{i}_{p1} \\ \dot{i}_{p2} \\ \vdots \\ \dot{i}_{pn} \\ \dot{i}_s \end{bmatrix} \tag{1}$$

where $R_o = 8R_L/\pi^2$, D_n is determined by the duty cycle of the buck-boost converter at the primary side, and $u_n = D_n/(1-D_n)^* U_{inn}$. Without loss of generality, the parameters of two excitation units are symmetric, that is, $L_{p1} = L_{p2} \ldots = L_{pn} = L_p$, $C_{p1} = C_{p2} \ldots = C_{pn} = C_p$, $R_{p1} = R_{p2} \ldots = R_{pn} = R_p$,.

Taking two adjacent excitation unit coils which are the same size with 10cm radius as an example, the coupling

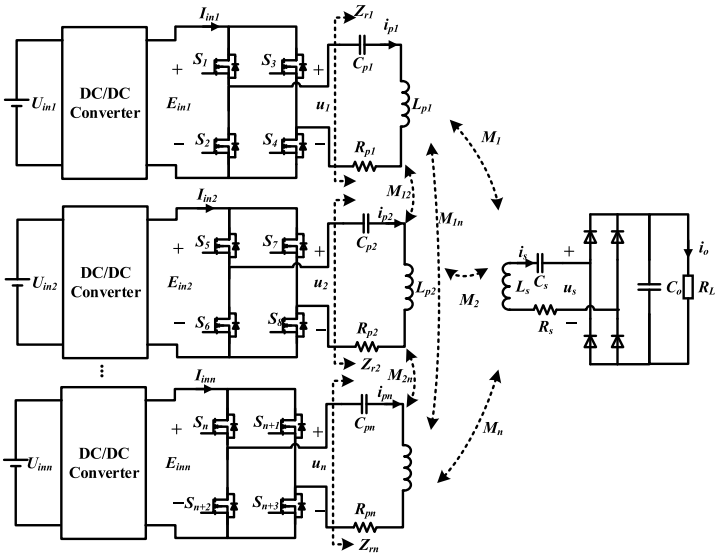

FIGURE 2. Equivalent circuit model of the MEU-WPT system.

coefficient curve of two coils is shown in Fig. 3. It can be seen that the cross coupling is very small when two coils are placed on the same horizontal plane (where x = 0.21or −0.21) and the distance between coils is 1 cm.

Under this condition of no overlapping area, to minimize the influence of cross-coupling, the primary and pick-up side operate at an identical angular frequency ω, given by:

$$\omega = \frac{1}{\sqrt{L_s C_s}} = \frac{1}{\sqrt{L_p C_p}} \tag{2}$$

For simplification of the equation, when the transmitting coil is distributed in the same plane, the cross coupling is far less than mutual inductance. And substituting (2) into (1), the resonant current i_{p1}, i_{p2}, i_{p3} can be derived by

$$\begin{cases} \dot{i}_{p1} = \dfrac{R_p(R_o+R_s)u_1 + \omega^2(u_1\sum_{i=1}^{n} M_i^2 - M_1\sum_{i=1}^{n} M_i u_i)}{R_p^2(R_o+R_s) + \omega^2 R_p \sum_{i=1}^{n} M_i^2} \\ \dot{i}_{p2} = \dfrac{R_p(R_o+R_s)u_2 + \omega^2(u_2\sum_{i=1}^{n} M_i^2 - M_2\sum_{i=1}^{n} M_i u_i)}{R_p^2(R_o+R_s) + \omega^2 R_p \sum_{i=1}^{n} M_i^2} \\ \vdots \\ \dot{i}_{pn} = \dfrac{R_p(R_o+R_s)u_n + \omega^2(u_n\sum_{i=1}^{n} M_i^2 - M_n\sum_{i=1}^{n} M_i u_i)}{R_p^2(R_o+R_s) + \omega^2 R_p \sum_{i=1}^{n} M_i^2} \\ \dot{i}_s = \dfrac{\omega\sum_{i=1}^{n} M_i u_i}{R_p(R_o+R_s) + \omega^2 \sum_{i=1}^{n} M_i^2} \end{cases} \tag{3}$$

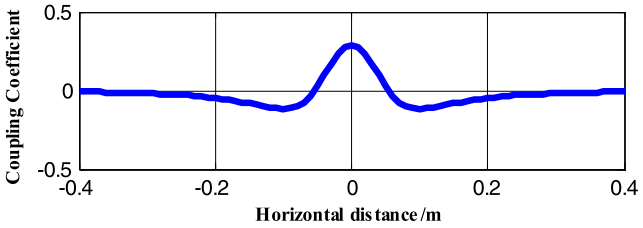

FIGURE 3. Cross coupling curve with two same coils.

The function of the power loss P_{loss} in the MEU-WPT system can be expressed as

$$P_{loss} = R_p \sum_{i=1}^{n} i_p^2 + R_s i_s^2 \tag{4}$$

Considering the losses of resistance R_p and R_s, the system's efficiency can be obtained as:

$$\eta = \frac{R_p \sum_{i=1}^{n} i_p^2 + R_s i_s^2}{R_p \sum_{i=1}^{n} i_p^2 + R_s i_s^2 + P_{out}} \tag{5}$$

III. COUPLING AREA ANALYSIS OF THE MEU-WPT SYSTEM

In the charging process, the output ability of the current position can be determined according to the position of the secondary coil. Study [22] proposed a method to determine the charging area and establish whether the location satisfies the charging requirements. However, when the secondary coil is located in the charging area, it is necessary to determine whether it is in the optimal charging area or a weakly coupling area to implement an optimal power distribution strategy. As such, the area adaption method is highlighted in this report. As shown in Fig. 4, the rated power is set to 100 W, and the

green area is the optimal charging area while the blue area is the weakly coupling area.

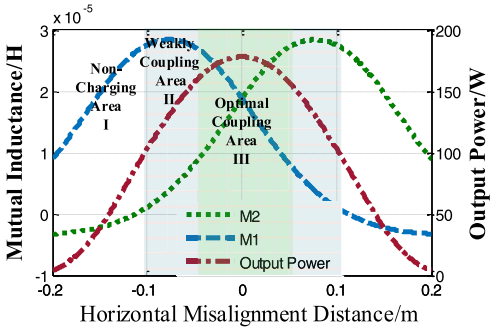

FIGURE 4. Charging area distribution diagram.

A. ANALYSIS OF OPTIMAL COUPLING AREA

To realize coupling area division, it is important to define the division criteria for the optimum coupling and the weakly coupling areas. The optimum coupling area can be given as

$$\begin{aligned} P_{position} &\geq P_{target} \\ \eta_{position} &\geq \eta_{target} \end{aligned} \tag{6}$$

where $P_{position}$ is the output power at any position of the three-dimensional coordinate system, and P_{target} is the objective of the output power. Fig. 5 shows the optimal coupling area. In this area, the power transfer capability is much higher than the output power requirement, and the system efficiency is the major target to achieve the best system performance.

To achieve maximum efficiency of the MEU-WPT system, a tracing strategy based on input power control is required. This method is implemented by tracking the minimum input power while maintaining the output at the required power. Considering the losses of the coupling mechanism, substituting (3) into (4), the equation can be expressed as follows:

$$\begin{aligned} P_{loss} = f(u_1, u_2 \dots u_n) &= \frac{\omega^2 R_s g(u_1, u_2 \dots u_n)^2}{\left[R_p(R_o + R_s) + \omega^2\alpha\right]^2} \\ &+ \frac{R_p^2(R_o + R_s)^2 h(u_1, u_2 \dots u_n) + \omega^4[\alpha^2 h(u_1, u_2 \dots u_n) - \alpha g(u_1, u_2 \dots u_n)^2]}{R_p\left[R_p(R_o + R_s) + \omega^2\alpha\right]^2} \\ &+ \frac{+2R_p(R_o + R_s)\omega^2[\alpha h(u_1, u_2 \dots u_n) - g(u_1, u_2 \dots u_n)^2]}{R_p\left[R_p(R_o + R_s) + \omega^2\alpha\right]^2} \end{aligned} \tag{7}$$

where

$$\begin{aligned} \alpha &= \sum_{i=1}^{n} M_i^2 \\ g(u_1, u_2 \dots u_n) &= \sum_{i=1}^{n} M_i u_i \\ h(u_1, u_2 \dots u_n) &= \sum_{i=1}^{n} u_i^2 \end{aligned} \tag{8}$$

To determine the maximum point of the n-variable functions, we set the first-order partial derivative of the function

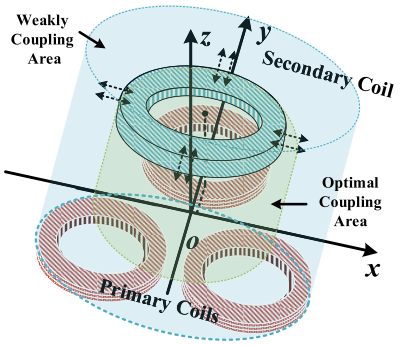

FIGURE 5. Optimal charging area of the MEU-WPT.

$f(u_1, u_2, \dots, u_n)$ equals to 0, which can be expressed as follows:

$$\begin{aligned} &\frac{\partial f(u_1, u_2 \dots u_n)}{\partial u_i} \\ &= 2\omega^2 R_s M_i g(u_1, u_2 \dots u_n) + 2R_p(R_o + R_s)^2 u_i \\ &\quad + \frac{\omega^4}{R_p}[2\alpha^2 u_i - 2\alpha M_i g(u_1, u_2 \dots u_n)] \\ &\quad + 2(R_o + R_s)\omega^2[2\alpha u_i - 2M_i g(u_1, u_2 \dots u_n)] = 0 \end{aligned} \tag{9}$$

From (9), the Hessian Matrix of $f(u_1, u_2, \dots, u_n)$ that is used to solve the extremum problem of a multivariate function, the second-order partial derivatives of $f(u_1, u_2, \dots, u_n)$ at u_i could be derived as:

$$A = \begin{bmatrix} f_{11} & f_{12} & \cdots & f_{1n} \\ f_{21} & f_{22} & \cdots & f_{2n} \\ \vdots & & \ddots & \vdots \\ f_{n1} & f_{n2} & \cdots & f_{nn} \end{bmatrix} \tag{10}$$

where the expression for an element of matrix A could be written as follows:

$$\begin{aligned} \frac{\partial^2 f}{\partial u_n^2} &= 2\omega^2 R_s M_n^2 + 2R_p(R_o + R_s)^2 \\ &\quad + \frac{2\omega^4}{R_p}(\alpha^2 - \alpha M_n^2) + 4(R_o + R_s)\omega^2(\alpha - M_n^2) \\ \frac{\partial^2 f}{\partial u_i \partial u_j} &= 2\omega^2 R_s M_i M_j - \frac{2\omega^4 \alpha M_i M_j}{R_p} - 4\omega^2 M_i M_j (R_o + R_s) \end{aligned} \tag{11}$$

In (10) and (11), it can be proved that the item containing ω^4 is the dominated part of the equation, with a range of valued from e^{24} to e^{32}. Other low-order items can be ignored without influencing the final results. Substituting (11) into (10), matrix A could be simplified as follows

$$A = \begin{bmatrix} \alpha - M_1^2 & -M_1 M_2 & \cdots & -M_1 M_n \\ -M_2 M_1 & \alpha - M_2^2 & \cdots & -M_2 M_n \\ \vdots & \vdots & \ddots & \vdots \\ -M_n M_1 & -M_n M_2 & \cdots & \alpha - M_n^2 \end{bmatrix} \tag{12}$$

Based on elementary row and column operations of matrix A, for simplification, this matrix can be transformed as (13), shown at the bottom of this page.

From (13), the eigenvalues of the Hessian matrix A are greater than or equal to zero, which means that the Hessian matrix A is a positive semi-definite matrix. According to the extremum theorem of multivariate functions, when the Hessian matrix of a function is a positive semi-definite matrix, value of $f(u_1, u_2, \ldots, u_n)$ (when $f'(u_1, u_2, \ldots, u_n) = 0$) is smaller than or equal to other points. As such, the function P_{loss} has a minimum value. When one of the value $u_j$is set, the points of efficiency maximum of function $f(u_1, u_2, \ldots, u_n)$ must converge to the function $G(u_1, u_2, \ldots, u_n)$ $(n \neq j)$. The relationship between u_j and other inputs $u_1, u_2 \ldots u_n$ $(n \neq j)$ could be expressed from (9)

$$u_j = G(u_1, u_2, \ldots, u_n)(n \neq j) = \frac{M_j \sum_{i=1, i\neq j}^{n} M_i u_i}{\sum_{i=1, i\neq j}^{n} M_i^2} \tag{14}$$

B. ANALYSIS OF WEAKLY COUPLING AREA

Based on the previous analysis, it is evident that the efficiency optimization of 3 excitation units could be achieved by adjustment of the DC input voltage. However, when the receiver moves close to the edge as shown in Fig. 6. The rated output power cannot be achieved for the condition of maximum efficiency tracking. In this mode, the satisfaction of the output power requirement is a prerequisite to maintain the operation of a normal system.

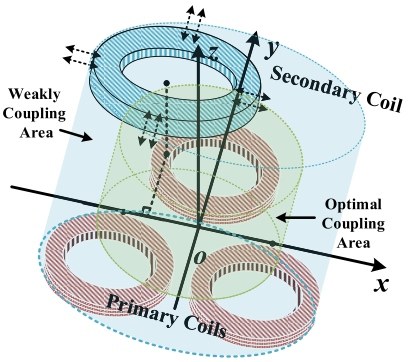

FIGURE 6. Weakly coupling area of MEU-WPT.

According to (6), the system in a weakly coupling area could be described as follows:

$$\begin{aligned} P_{position} &\geq P_{t\,\arg et} \\ \eta_{position} &< \eta_{t\,\arg et} \end{aligned} \tag{15}$$

From (15), the optimization target of efficiency is not considered, because it is difficult to satisfy the rated power. From (4), the output power can be simplified as

$$\begin{aligned} P_{out} &= \left(\frac{\omega R_p (R_o + R_s) g(u_1, u_2 \ldots u_n)}{R_p^2 (R_o + R_s) + \omega^2 R_p g(u_1, u_2 \ldots u_n)}\right)^2 / R_o \\ P_{out} &\propto g(u_1, u_2 \ldots u_n) \end{aligned} \tag{16}$$

As such, from the preceding equation (16) can be seen, the output power is proportional to $g(u_1, u_2, \ldots u_n)$. Therefore, to reach the rated power, the function$g(u_1, u_2, \ldots u_n)$ of a weakly coupling area condition only needs to satisfy the

$$\begin{aligned} A &\sim \begin{matrix} -\frac{M_1}{M_n} r_n + r_1 \\ \vdots \\ -\frac{M_{n-1}}{M_n} r_n + r_{n-1} \end{matrix} \begin{bmatrix} \alpha & 0 & \cdots & 0 & -\frac{M_1}{M_n}\alpha \\ 0 & \alpha & \cdots & 0 & -\frac{M_2}{M_n}\alpha \\ \vdots & \vdots & \ddots & \vdots & \vdots \\ 0 & 0 & 0 & \alpha & -\frac{M_{n-1}}{M_n}\alpha \\ -M_n M_1 & -M_n M_2 & \cdots & -M_n M_{n-1} & \alpha - M_n^2 \end{bmatrix} \\ &\sim \begin{matrix} \frac{M_1}{M_n} c_1 + c_n \\ \vdots \\ \frac{M_{n-1}}{M_n} c_{n-1} + c_n \end{matrix} \begin{bmatrix} \alpha & 0 & \cdots & 0 & 0 \\ 0 & \alpha & \cdots & 0 & 0 \\ \vdots & \vdots & \ddots & \vdots & \vdots \\ 0 & 0 & 0 & \alpha & 0 \\ -M_n M_1 & -M_n M_2 & \cdots & -M_n M_{n-1} & \alpha - \sum_{i=1}^{n} M_n^2 \end{bmatrix} \\ &= \begin{bmatrix} \alpha & 0 & \cdots & 0 & 0 \\ 0 & \alpha & \cdots & 0 & 0 \\ \vdots & \vdots & \ddots & \vdots & \vdots \\ 0 & 0 & 0 & \alpha & 0 \\ -M_n M_1 & -M_n M_2 & \cdots & -M_n M_{n-1} & 0 \end{bmatrix} \end{aligned} \tag{13}$$

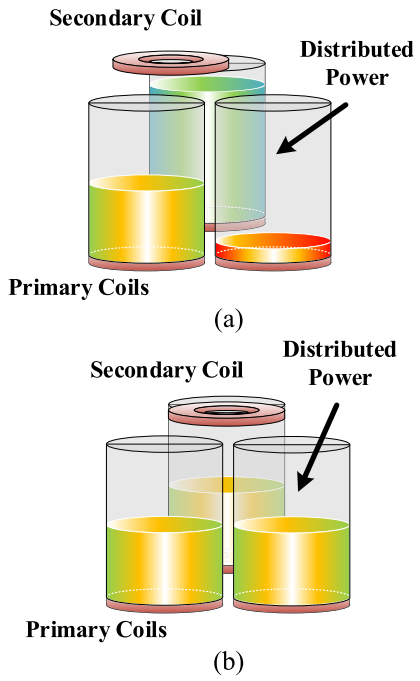

FIGURE 7. Cooperative control in different mode. (a) PR mode; (b) EO mode.

following:

$$\sum_{i=1}^{n} M_i u_i \geq \frac{P_{target} R_o [R_p^2 (R_o + R_s) + \omega^2 R_p \sum_{i=1}^{n} M_i^2]^2}{\omega^2 R_p^2 (R_o + R_s)^2} \quad (17)$$

IV. COOPERATIVE CONTROL DESIGN FOR THE MEU-WPT SYSTEM

To develop a system with environmental sensing capability and a smart distribution strategy, a cooperative control strategy is proposed as shown in Fig 7. In the different charging areas, the strategy for power distribution is different. An efficiency optimization mode (EO mode) was designed for the optimal coupling area and a power reaching mode (PR mode) was developed for the weakly coupling area. In the PR mode, to allow the system to achieve the rated power, the transmitters with large mutual inductance values are considered to transfer maximum power, while the excitation power of the transmitters with small mutual inductances is reduced. In the EO mode, the excitation power of every unit is modulated in balance so that the system achieves the rated power via efficiency optimization. According to the previous analysis, in cooperative control, it is necessary to dynamically obtain multiple coupling parameters among the multiple excitation units because the controller must distribute the excitation power of each unit dynamically, according to its coupling condition with the receiver. In this section, a coupling parameter identification method is proposed. For simplicity, a dual excitation unit WPT system is considered as an example.

Fig. 8 shows the control scheme for the proposed system.

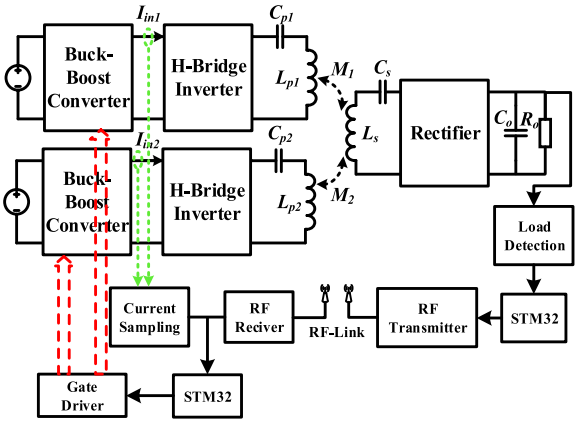

FIGURE 8. Control scheme for the proposed system.

A. COUPLING PARAMETERS IDENTIFICATION METHOD

In the receiver moving process, the coupling parameters undergo a fast and dramatic variation. It is a significant challenge to realize fast parameter identification in a short period. Traditional identification methods may exhibit multiple solution problems [15], [22]–[26]. This report outlines a multiple coupling identification method based on multiple DC input information. Its main advantage is that multiple solution problems are not encountered, which greatly enhances the response speed in terms of identifying real solutions. Furthermore, given that only DC variables are considered, this method is easily implemented.

The output voltage $U_{DC-conver\_n}$ of converter could be expressed as $U_{DC-conver\_n} = U_{in\_n}{}^* D_n/(1 - D_n)$. And the relationship between full-bridge inverter input voltage $U_{DC-conver\_n}$ and output voltage could be expressed as $E_{in\_n} = 2\sqrt{2}U_{DC\_converter\_n}/\pi$. Therefore, the input voltage of the inverter could be expressed as

$$\frac{2\sqrt{2}D_n U_{in\_n}}{\pi(1 - D_n)} = E_{in\_n} \quad (18)$$

where D_n is determined by the duty cycle of the DC-DC converter at the primary side. For each single excitation unit, according to the power conservation $E_{in\_n^*} I_{in\_n} = u_n^* i_{pn}$, the DC bus current of voltage-source inverter I_{in_n} is close to the RMS value of the output current i_n of the inverter, which could be expressed as $I_{in\_n} = 0.9 i_{pn}$. Moreover, given that the load values can be measured and communication is used. Because the system parameters R_s, R_{pn} and u_n are known, the function $i_{pn} = f_n(M_1, M_2, \ldots, M_n)$ between the current of the resonant network and the equivalent reflection impedance can be obtained with (3). The result shows the dynamic change of misalignment. There are n equations and n variables. To obtain the solution for mutual inductance, it is only necessary to detect the current of the primary side. The output of inverters could be obtained as follows:

$$i_{p1} = \frac{b u_1 + \omega^2 M_2 (M_2 u_1 - M_1 u_2)}{R_p (a + b)}$$

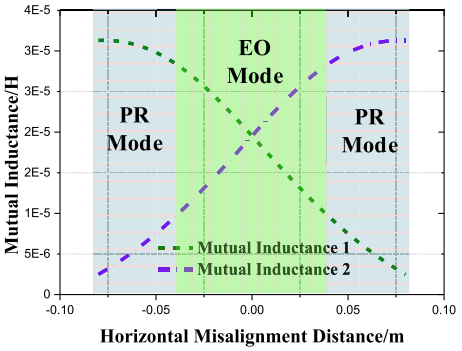

FIGURE 9. The curve of λ under variation of mutual inductance.

$$i_{p2} = \frac{bu_2 + \omega^2 M_1(M_1u_2 - M_2u_1)}{R_p(a+b)} \tag{19}$$

where $a = (M_1^2 + M_2^2)\omega^2$, and $b = (R_s + R_o)R_p$. Substituting (18) into (19), the mutual inductance could be obtained as

$$\begin{aligned} \mathrm{M}_1 &= \pm\frac{R_o(i_{p1}R_p - u_1)}{\omega\sqrt{-R_o\left[(i_{p1}^2 + i_{p2}^2)R_p - i_{p1}u_1 - i_{p2}u_2\right]}} \\ M_2 &= \pm\frac{R_o(i_{p2}R_p - u_2)}{\omega\sqrt{-R_o\left[(i_{p1}^2 + i_{p2}^2)R_p - i_{p1}u_1 - i_{p2}u_2\right]}} \end{aligned} \tag{20}$$

From (20), it is evident that there are two complementary roots of the equations, however, it is obvious that only positive value is acceptable. The polynomial in the denominator can be expressed as the difference between the losses for the primary coils $(i_{p1}^2 + i_{p2}^2)R_p$ and the input power $i_{p1}u_1$, $i_{p2}u_2$.

$$(i_{p1}^2 + i_{p2}^2)R_p - i_{p1}u_1 - i_{p2}u_2 \le 0 \tag{21}$$

Evidently, equation (21) must be less than or equal to 0. Similarly, $i_{p1}R_p - u_1$ *or* $i_{p2}R_p - u_2$ should also be less than or equal to 0. Therefore, the unique value of the mutual inductance could be determined. Equation (20) can be re-expressed as (22), shown at the bottom of this page.

B. COOPERATIVE CONTROL IN THE EO MODE

Fig. 9. shows the mutual inductance curve of the DEU-WPT system (the parameters refer to Table 1 in section IV) with misalignment. The relationship of varying mutual inductance reflects the relationship between two regulated voltages.

In Fig. 9, the ratio value of mutual inductance for the EO mode is not large, so that the regulated voltage is easy to achieve. For the DEU-WPT system, from (14), it is proved

TABLE 1. The main parameter of system.

Parameters	Values	Patameters	Values
L_{p1}/L_{p2}	100μH	L_s	210μH
R_p	0.15Ω	R_s	0.3Ω
C_{p1}/C_{p2}	31.27nF	C_s	14.89nF
z	6cm	d_r	1cm
M_{12}	0.2μH	R_L	10Ω

that the function of losses has a minimum value. The relationship between two the input voltage could be obtained based on the following equations:

$$\begin{aligned} u_{1\_EO\ \mathrm{mode}} &= \frac{\omega^2 M_1 M_2(a - R_pR_s + 2b)u_2}{\omega^2 M_2^2 a + \omega^2 M_1^2 R_pR_s + 2\omega^2 M_2^2 b + b^2} \\ u_{2\_EO\ \mathrm{mode}} &= \frac{\omega^2 M_1 M_2(a - R_pR_s + 2b)u_1}{\omega^2 M_1^2 a + \omega^2 M_2^2 R_pR_s + 2\omega^2 M_1^2 b + b^2} \end{aligned} \tag{23}$$

where $a = (M_1^2 + M_2^2)\omega^2$, and $b = (R_s + R_o)R_p$. Similarly, we can simplify the preceding equations. The relationship between the input voltage of two primary coils can be expressed as

$$\begin{aligned} u_{1\_EO\ \mathrm{mode}} &= \frac{M_1}{M_2}u_{2\_EO\ \mathrm{mode}} = \lambda u_{2\_EO\ \mathrm{mode}} \\ u_{2\_EO\ \mathrm{mode}} &= \frac{M_2}{M_1}u_{1\_EO\ \mathrm{mode}} = \frac{1}{\lambda}u_{1\_EO\ \mathrm{mode}} \end{aligned} \tag{24}$$

Using (24), we can distribute the input power by changing the value of u_1 and u_2 to achieve the required output power. In addition, when u_1 and u_2 satisfy the preceding expression, the efficiency could be optimal. In the EO mode, due to the proportional relationship between the voltages based on the optimal efficiency analysis, an equation with one variable can be established to solve for the value of the input voltage, which can be expressed as

$$\begin{aligned} u_{1\_EO\ \mathrm{mode}} &= \frac{[R_p^2(R_o+R_s) + \omega^2 R_p(M_1^2 + M_2^2)]\sqrt{P_{target}R_o}}{\omega R_p(R_o + R_s)M_1(1/\lambda^2 + 1)} \\ u_{2\_EO\ \mathrm{mode}} &= \frac{[R_p^2(R_o+R_s) + \omega^2 R_p(M_1^2 + M_2^2)]\sqrt{P_{target}R_o}}{\omega R_p(R_o + R_s)M_2(\lambda^2 + 1)} \end{aligned} \tag{25}$$

C. COOPERATIVE CONTROL IN THE PR MODE

However, in the PR mode, from Fig. 9, it is evident that the ratio value of mutual inductance is much greater than that of the EO mode. For example, for x = 0.08 m, the λ (M_1/M_2) is almost equal to 10. Under this condition, if the system operates in the EO mode, u_2 will be very small even though u_1 maintains the maximum input value u_{max}. Therefore, to guarantee the output power, the other input voltage

$$\begin{aligned} \mathrm{M}_1 &= \frac{R_o(1.1\bar{I}_{in1}R_p - 0.9\bar{E}_{in1})}{\omega\sqrt{-R_o\left[(1.1\bar{I}_{in1}^2 + 1.1\bar{I}_{in2}^2)R_p - 1.1\bar{I}_{in1}0.9\bar{E}_{in1} - 1.1\bar{I}_{in2}0.9\bar{E}_{in2}\right]}} \\ M_2 &= \frac{R_o(1.1\bar{I}_{in2}R_p - 0.9\bar{E}_{in2})}{\omega\sqrt{-R_o\left[(1.1\bar{I}_{in1}^2 + 1.1\bar{I}_{in2}^2)R_p - 1.1\bar{I}_{in1}0.9\bar{E}_{in1} - 1.1\bar{I}_{in2}0.9\bar{E}_{in2}\right]}} \end{aligned} \tag{22}$$

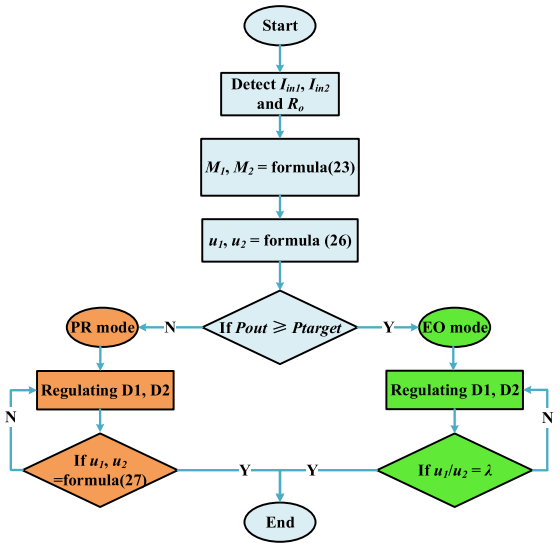

FIGURE 10. Flow chart of control.

could be obtained as

$$u_{1\_PR\ mode} = u_{\max}$$

$$u_{2\_PR\ mode} = \frac{[R_p^2(R_o + R_s) + \omega^2 R_p(M_1^2 + M_2^2)]\sqrt{P_{t\,arg\,et} R_o}}{\omega R_p(R_o + R_s)M_2^2} - \lambda u_{\max} \quad (26)$$

D. SWITCHING CONTROL STRATEGY OF THE DEU-WPT SYSTEM

With the coupling observation from (22), the cooperative control for efficiency optimization and power supply in different charging area can be implemented by distributing the power among multiple excitation units. According to the mutual inductance observation, I_{in1}, I_{in2}, and D_1, D_2 are used to calculate mutual inductance, while the load R_L could be determined using U_o and I_o. The regulated voltage could be determined from (26) or (25). Fig. 10 shows the control flow, which can be given as follows:

1) System works normally and the duty cycles D_1, D_2 are fixed at an initial value.
2) To observe the coupling coefficients dynamically, the input current and load are detected. The real-time values of mutual inductance are calculated using equations (22).
3) Substituting the ratio value of the voltage into (25), and input power could be modulated
4) Determine whether the output power reaches the target value. If yes, go to the EO mode. If not, go to the PR mode.
5) Compare the state of the output power with the target state, and regulate the duty cycle D_1 and D_2 to reduce the error.

V. PERFORMANCE ANALYSIS AND EXPERIMENT RESULTS

To verify the proposed method, simulation and experimental systems were built with cross coupling considered. The primary coils were placed in parallel to reduce cross-coupling. The system's operating frequency was set to $f = 90$ kHz, and the load was $R_L = 10\ \Omega$. According to (2), the other parameters are listed in Table 1. d_r is horizon direction and the z is the transmission height.

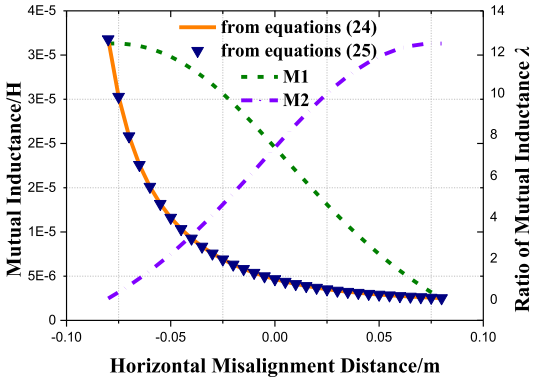

FIGURE 11. Curve of λ under variation of mutual inductance.

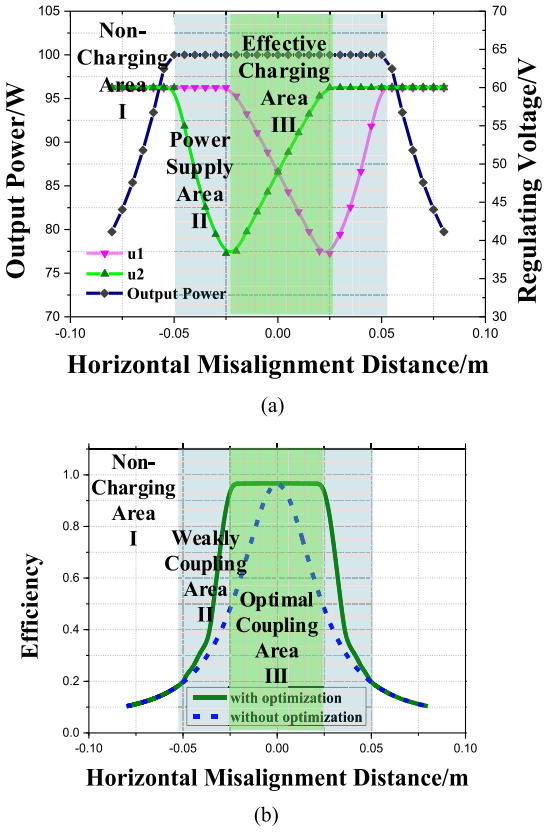

FIGURE 12. Output characteristics with efficiency optimization control. (a) Curve of input voltage regulation and output power. (b) Comparison of efficiency curve.

A. SIMULATION ANALYSIS

Fig. 11. shows the curve for the ratio $\lambda(\lambda = M_1/M_2)$ with misalignment. The horizontal ordinate is the horizontal misalignment distance, the left longitudinal coordinate is the value of the mutual inductance, and the right is the ratio λ.

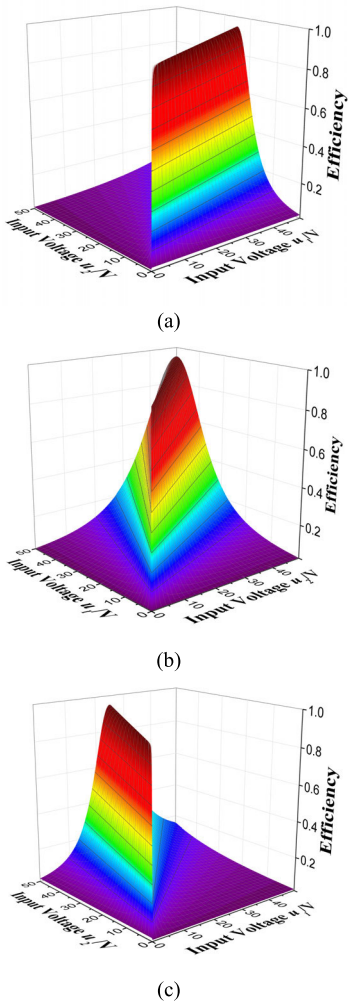

FIGURE 13. Efficiency under modulation of input voltage. (a) $\lambda = 2$. (b) $\lambda = 1$. (c) $\lambda = 0.5$.

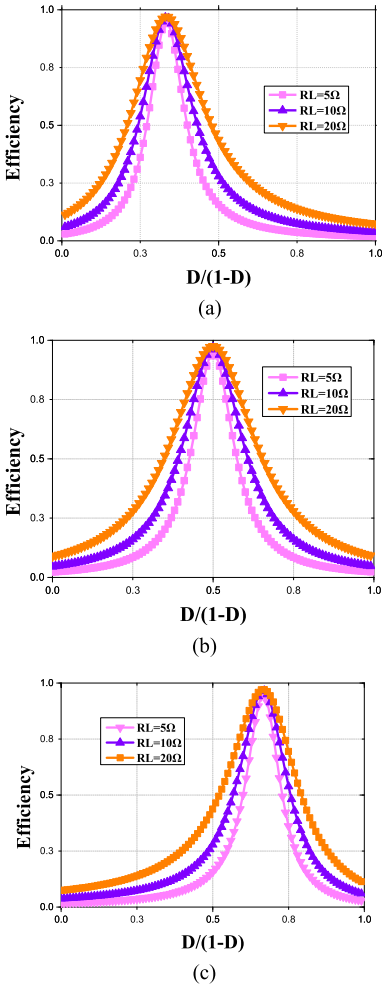

FIGURE 14. Efficiency curve under variation of the load. (a) $\lambda = 2$. (b) $\lambda = 1$. (c) $\lambda = 0.5$.

The olive and violet curves represent the mutual inductance values. The orange curve is the simulation value of λ, and the navy symbols represent the calculated ratio obtained from equation (24).

It is evident in Fig. 11 that the simulation (blue symbol curve) is consistent with the theoretical results (orange curve). As such, the ratio (M_1/M_2) of the two mutual inductances is consistent with the input voltage ratio (u_1/u_2). This result that verifies the simplified maximum efficiency condition given by (24) is correct. However, λ is large in the weakly coupling area, and is almost greater than 10. Therefore, one of the modulated voltages could be very small. From Fig 11, it is evident that the EO mode may not be suitable for the entire charging area because the rated power may not be satisfied.

Fig. 12 shows the charging process for three different areas with two control modes. The input voltage range is set as 0 – 60 V, and the required output power is 100 W.

In Fig. 12, the output characteristics of the DEU-WPT system for optimal efficiency is achieved in the optimal coupling area (green space) by regulating the input voltages, while the rated power is maintained in the weakly coupling area (blue space). From Fig. 12, it is evident that it can be divided into 3 parts according to different horizontal misalignments.

Part I is the non-charging area. All DC-DC circuits output 60 V, because the maximum input voltage does not allow the output to achieve the rated power.

Part II is the weakly coupling area based on PR mode control. Once the output power reaches the required power, the system enters the charging area. At this time, if the input voltage ratio is satisfied, the output power may not reach the rated power. Therefore, to satisfy the output power requirement, it should take precedence over maximum efficiency tracking. In this area, the input of the excited coils with a large mutual inductance will be maintained at the maximum value of the DC-DC module. In Fig. 12, M_1 is greater than M_2 in this area, therefore, u_1 will be maintained at 60 V and u_2 will be regulated so that the ratio of the input voltage could be close to λ.

Part III is the optimal coupling area based on efficiency optimization mode control. Using the tracking control method mentioned, the efficiency of the system could be kept at a high value. In Fig. 12 (b), compared with the efficiency in

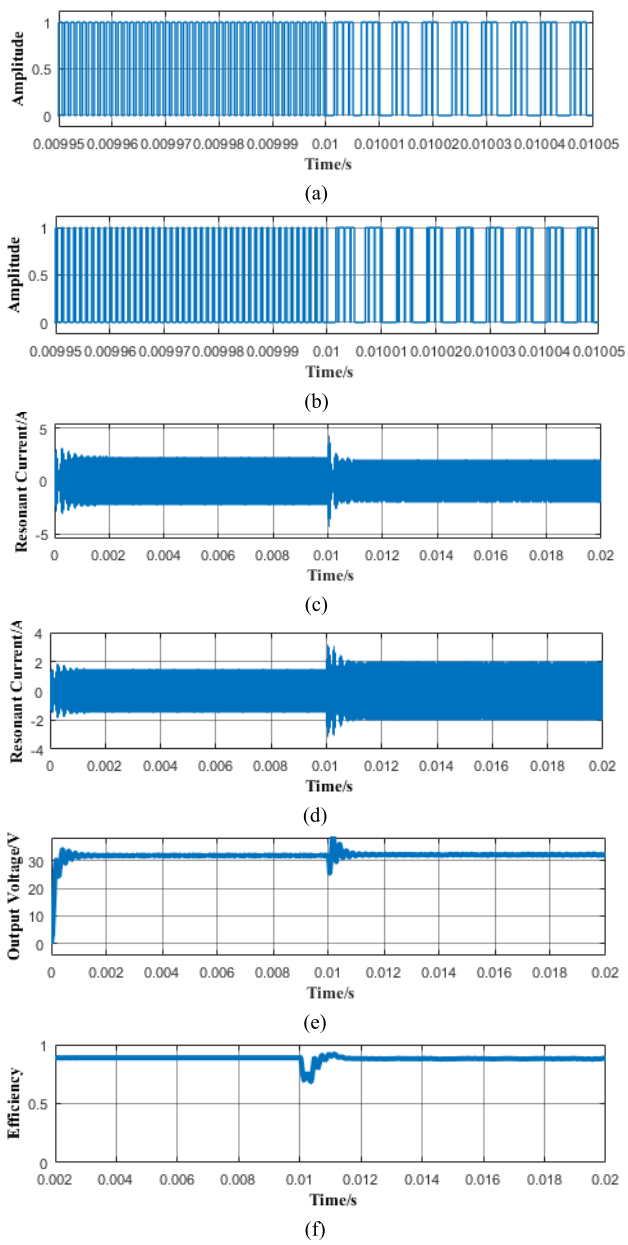

FIGURE 15. Waveform of the mode switched. (a) Duty-cycle of buck-boost converter 1. (b) Duty cycle of buck converter 2. (c) Resonant current of primary coil 1. (d) Resonant current of primary coil 2. (e) Output voltage curve of the load. (f) Efficiency curve.

the absence of optimization, it is evident that the DEU-WPT system has a large efficiency improvement.

In Fig. 13. (a), the ratio of u_1 and u_2 at maximum efficiency is 0.5. Similarly, in Fig. 13. (b) and (c), the ratio of u_1 and u_2 at maximum efficiency is almost the same as the ratio of mutual inductance λ. However, the SS-type system is sensitive to parameter variations so that the efficiency surface appears to be steep. To solve this problem, tracking control could be added to keep the resonant current of primary coils constant, or to replace resonant topology with composite resonance such as LCL (Inductance - Capacitor - Inductance) or LCC (Inductance – Capacitor - Capacitor).

Considering the variation of the load, the efficiency curve of DEU-WPT is shown in Fig. 14. The abscissa is the ratio D/(1-D) of the output voltage to the input voltage of the DC-DC circuit in one of the excitation units u_1, when the other input voltage u_2 is set.

From Fig. 14, there are three cases when the ratio λ is different for a change of the load. When $\lambda = 2$, the duty cycle is almost stable at 1/3, so that D/(1-D) = 0.5, and the ratio of the input power could be consistent with the mutual inductance. Moreover, the efficiency could be a maximum when the load changes. Similarly, from Fig. 14. (b) and (c), the theoretical analysis was verified.

Fig. 15 shows the waveform of the system when the mode switched. Before 0.01 s, the system operated under the condition that the ratio (M_1/M_2) of two mutual inductances is 2. At the time 0.01 s, the ratio (M_1/M_2) of the two mutual inductance values change to 1.

In Fig. 15 (a) and (b) shows the modulation of the duty cycle of each converter. In the steady-state of the system in the first coupling case, the ratio of the duty cycle almost satisfies equations (24). In addition, the output power is maintained at 100 W from Fig. 15 (e). At the time 0.01 s, the coupling condition changes. From Fig. 15 (c) (d) (e) and (f), the response time is almost 1 ms. Fig. 15 (c) and (d) show that the resonant current changes with the converter modulation. After input voltage modulation in the second coupling case, the output power is maintained at 100 W and the efficiency maintains a high value of almost 93 %.

Fig. 16 shows the improvement of the efficiency of the proposed control method under different coupling conditions. In Fig 16. (a) and (b), the ratio (M_1/M_2) of two mutual inductances is 2. In Fig. 16 (c) and (d), the ratio (M_1/M_2) of two mutual inductances is 1. Prior to 0.01 s, the system maintained a constant output when the proposed method was not used. However, after 0.01 s, the proposed method was used.

From Fig. 16 it is evident that under different coupling conditions, the proposed method can improve the efficiency by providing a better power distribution strategy when the output power is maintained.

B. EXPERIMENTAL RESULTS

An image of the DEU-WPT experimental device is shown in Fig. 17. The system's operating frequency f is set as 90 kHz, and the load R_L is 10 Ω. The other parameters are given in Table 1.

The design parameters of coupling structure are shown in the Table 2, where N is the turns of coil. r_{min} is the inner diameter of coil. d_{coil} is diameter of wire. c is the layers number of coil. g is the wire spacing. Two primary coils are placed tightly at horizon direction d_r which is 1cm. And the the transmission height z is 0.06m.

To verify that the maximum efficiency was achieved, two situations of mutual inductance variation switching testing were conducted. The experimental test diagram is shown in Fig. 18.

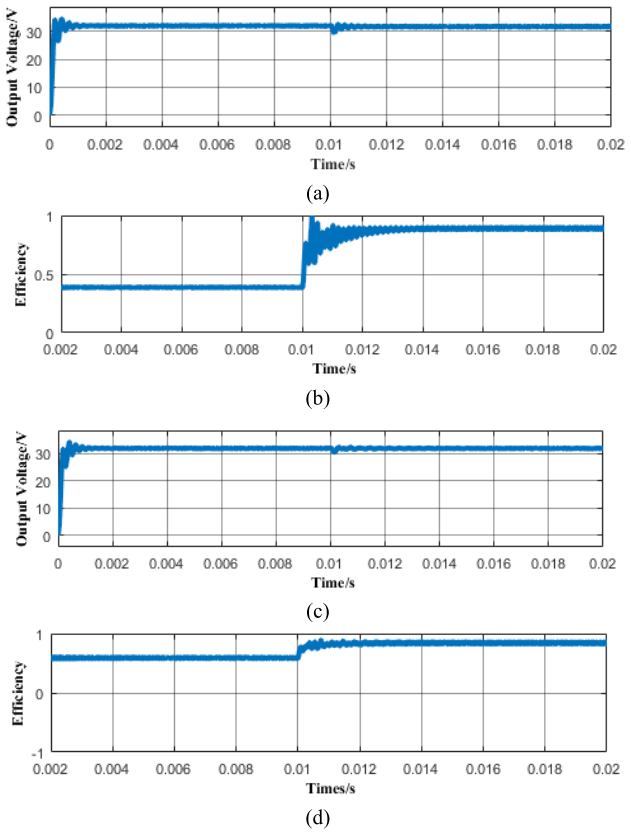

FIGURE 16. Output waveform with the proposed control method (or without proposed control method). (a) Output voltage when M1:M2 = 1. (b) Efficiency when M1:M2 = 1. (c) Output voltage when M1:M2 = 2. (d) Efficiency when M1:M2 = 2.

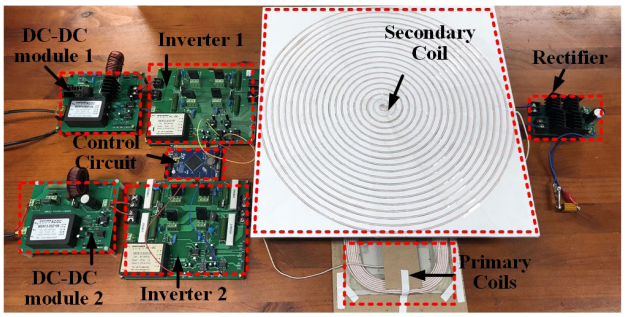

FIGURE 17. Experimental setup.

With specific design parameters of coils in Table 2. There are two cases of secondary coil position are tested in experiment as shown in Fig. 18. In case one, the secondary coil is placed on the center of two excitation units, where $x_0 = 0$m, $y_0 = 0$m and $z_0 = 0.06$m. In case two, the secondary coil is moved to another position quickly, where $x_1 = 0.02$m, $y_1 = 0$m and $z_1 = 0.06$m.

Fig. 19 shows wireless charging with loose coupling. In this case, $M_1 = 20\ \mu$H, $M_2 = 20\ \mu$H. In Fig. 19., to distinguish the efficiency between the relationship of the two situation, U_{in2} and U_{in1} are regulated to reach rated power 100 W. Initially, before optimization, the input voltage U_{in1} is 75 V and U_{in2} is 39.1 V. And the RMS values of resonant

TABLE 2. The parameter of coils design.

Symbol	Primary Coil	Secondary Coil
N	10	20
r_{min}	0.06m	0.01m
d_{coil}	0.002m	0.003m
c	3	2
g	0.002m	0.01m

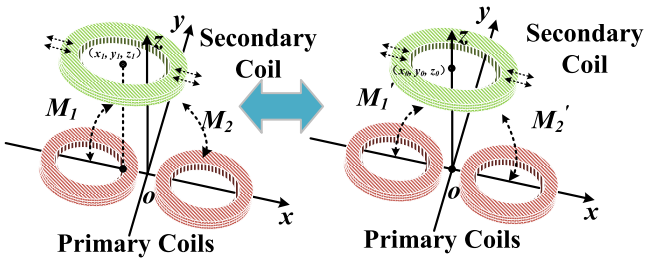

FIGURE 18. Experimental test diagram.

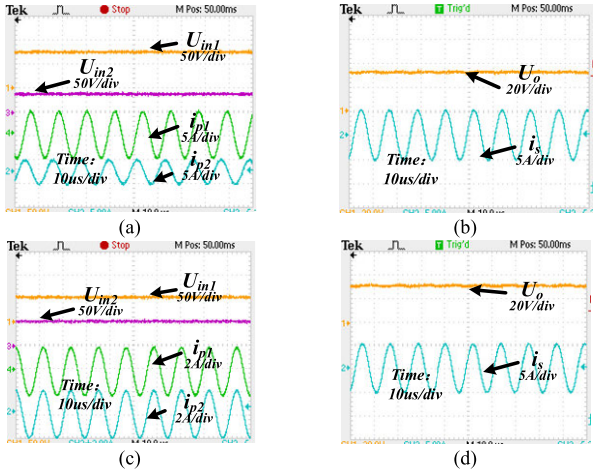

FIGURE 19. Experimental results with loose coupling when M1 = M2 = 20μH. (a) Waveform in primary side before control. (b) Waveform in secondary side before control. (c) Waveform in primary side after control. (d) Waveform in secondary side after control.

current i_{p1} is 3.3A while the i_{p2} is 1.78A. At secondary side, the output voltage U_o is 31.6V and RMS values of resonant current i_s is 3.54A. It is evident that there is a phase difference, and the efficiency is 35%. After optimization control, the system reaches the state of maximum efficiency, U_{in2} and U_{in1} reaches 52 V and 52.4 V. i_{p1} is and i_{p2} is 1.34A when the efficiency is 80 % when the rated power is kept. The current phase is the same and the ratio of the voltage is equal to the $\lambda = 1$.

In the case of Fig. 20, $M_1 = 26.02\ \mu$H, and $M_2 = 13\ \mu$H. The cross-coupling is 0.002. In Fig. 20. (a) and (b), U_{in1} is 70 V and U_{in2} is 25.3 V while the RMS values of i_{p1} is 2.48A and the i_{p2} is 1.13A. And the efficiency is 55.6 %. After reaching the steady-state with the controller, U_{in1} is modulated to 63.5 V and U_{in2} is 30V. The i_{p1} is 1.56A and the i_{p2} is 1.1A when the efficiency reaches 84 %.

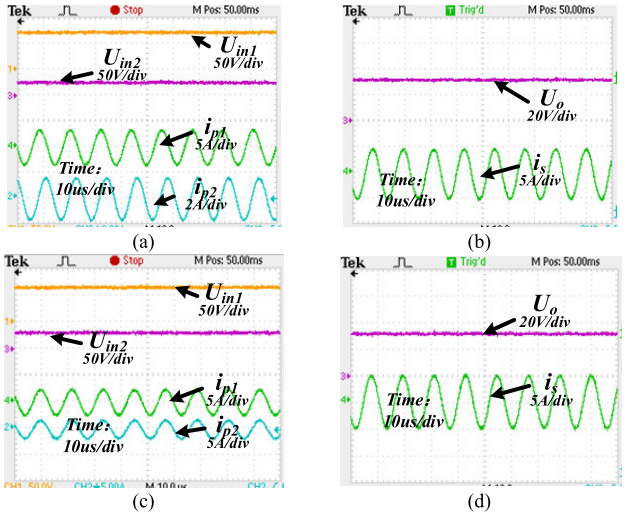

FIGURE 20. Experimental results with loose coupling when M1 = 26μH, M2 = 13μH. (a) Waveform in primary side before control. (b) Waveform in secondary side before control. (c) Waveform in primary side after control. (d) Waveform in secondary side after control.

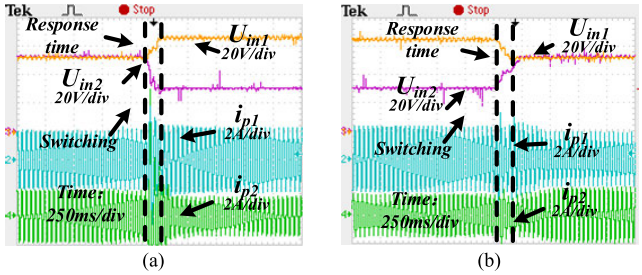

FIGURE 21. Experimental results with coupling variation. (a) M1 = M2 = 20μH change to M1 = 26μH, M2 = 13μH (b) M1 = 26μH, M2 = 13μH change to M1 = M2 = 20μH.

Fig. 21 shows the experimental results for coupling variation. Fig. 21 (a) shows the switching control when $M_1 = M_2 = 20\mu$H change to $M_1 = 26\mu$H, $M_2 = 13\mu$H, and Fig. 21 (b) shows the switching control when $M_1 = 26\mu$H, $M_2 = 13\mu$H change to $M_1 = M_2 = 20\mu$H. It can be seen that the control results of steady state waveform satisfies the previous analysis.

Fig. 22 shows the experimental results for 400W system. Fig. 22 (a) and (b) shows the waveform when $M_1 = M_2 = 20\mu$H. U_{in1} is 134V and U_{in2} is 84V. And the RMS values of resonant current i_{p1} is 4.78A while the i_{p2} is 3.53A. At secondary side, the output voltage U_o is 63V and the efficiency is 47%. After optimization control, the system reaches the state of maximum efficiency, U_{in2} and U_{in1} reaches 91.3 V. i_{p1} is and i_{p2} is 2.54A when the efficiency is 90 %. The current phase is the same and the ratio of the voltage is equal to the $\lambda = 1$. Fig. 22 (c) and (d) shows the waveform when $M_1 = 26\mu$H, $M_2 = 13\mu$H. U_{in1} is 144V and U_{in2} is 51.7V. And the RMS values of resonant current i_{p1} is 4.38A while the RMS values of i_{p2} is 2.26A. At secondary side, the efficiency is 60.2%. After optimization control, the system reaches the state of maximum efficiency. U_{in1} is 124V and U_{in2} is 64V. And the RMS values of resonant current i_{p1} is 3.09A while the i_{p2} is 2.1 A. And the efficiency is 86%.

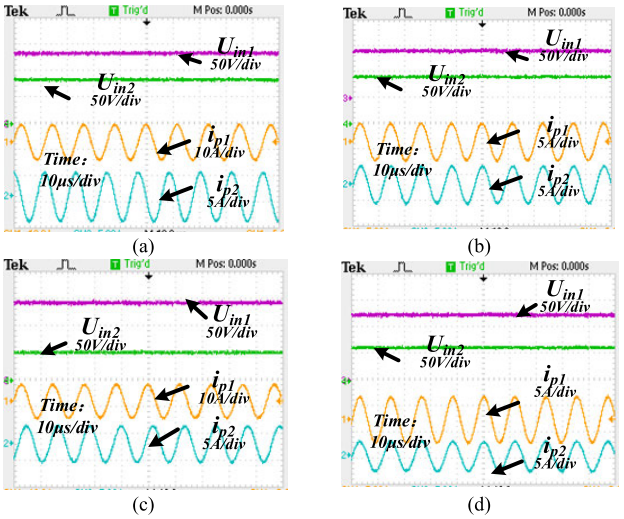

FIGURE 22. Experimental results with 400W system. (a) Waveform in primary side before control when M1 = M2 = 20μH. (b) Waveform in primary side after control when M1 = M2 = 20μH. (c) Waveform in primary side before control when M1 = 26μH, M2 = 13μH. (d) Waveform in primary side after control when M1 = 26μH, M2 = 13μH.

TABLE 3. The result of experiment.

Case	M_1 (µH)	M_2 (µH)	M_{12} (µH)	U_{in1} (V)	U_{in2} (V)	M_1/M_2	U_{in1}/U_{in2}	P_{out} (W)	η (%)
1 (before)	20	20	0.2	75	39.1	1	1.9	100	35
1 (after)	20	20	0.2	52.4	52	1	1	100	80
2 (before)	26	13	0.2	70	25.3	2	2.7	100	61.7
2 (after)	26	13	0.2	63.5	30	2	2.1	100	84
3 (before)	20	20	0.2	134	84	1	1.6	400	47
3 (after)	20	20	0.2	91.3	91.3	1	1	400	90
4 (before)	26	13	0.2	144	51.7	2	2.8	400	60.2
4 (after)	26	13	0.2	124	64	2	1.9	400	86

The experimental results in Table 3 validate the theoretical analysis, as shown in Table 4. The main factors that influence the efficiency are the inherent power losses on the circuit module and the existing errors in mutual inductance curve with math operation. Moreover, the system's efficiency can be improved using a better coil design. In addition, power loss can be reduced by replacement with a soft-switching buck converter.

VI. CONCLUSION

MEU-WPT technology provides a flexible solution for high power and large misalignment tolerance application. It can reduce cost and voltage stress in a single high-power unit. This report proposes a maximum efficiency tracking method for such a multiple excitation input-single pickup system. Moreover, this approach serves the dual objective of achiev-

TABLE 4. Comparison of simulation and experiment.

Case	M_1 (μH)	M_2 (μH)	U_{in1} (V)	U_{in2} (V)	M_1/M_2	U_{in1}/U_{in2}	P_{out} (W)
1 (simulation)	20	20	46	46	1	1	100
1 (experiment)	20	20	52.4	52	1	1	100
2 (simulation)	26	13	56	28	2	2	100
2 (experiment)	26	13	63.5	30	2	2.1	100
3 (simulation)	20	20	90	90	1	1	400
3 (experiment)	20	20	91.3	91.3	1	1	400
4 (simulation)	26	13	120	60	2	2	400
4 (experiment)	26	13	124	64	2	1.9	400

ing maximum efficiency tracking and output power control. In addition, an additional circuit is not required in the main topology, and only DC and duty cycle information are utilized. This method is simple and provide control design idea from DC bus. As such, it is suitable for the pickup of dynamical movement in the charging area of multiple excitation units. This method can be extended for use in other power electronic systems with parallel power sources.

REFERENCES

[1] Z. Zhang, A. Georgiadis, and C. Cecati, "Wireless power transfer for smart industrial and home applications," *IEEE Trans. Ind. Electron.*, vol. 66, no. 5, pp. 3959–3962, May 2019.

[2] A. Ramezani, S. Farhangi, H. Iman-Eini, B. Farhangi, R. Rahimi, and G. R. Moradi, "Optimized LCC-series compensated resonant network for stationary wireless EV chargers," *IEEE Trans. Ind. Electron.*, vol. 66, no. 4, pp. 2756–2765, Apr. 2019.

[3] X. Wang, Y. Wang, Y. Hu, Y. He, and Z. Yan, "Analysis of wireless power transfer using superconducting metamaterials," *IEEE Trans. Appl. Supercond.*, vol. 29, no. 2, Mar. 2019, Art. no. 5500605.

[4] Y. Tang, Y. Chen, U. K. Madawala, D. J. Thrimawithana, and H. Ma, "A new controller for bidirectional wireless power transfer systems," *IEEE Trans. Power Electron.*, vol. 33, no. 10, pp. 9076–9087, Oct. 2018.

[5] B. Zhao, N.-C. Kuo, and A. M. Niknejad, "A gain boosting array technique for weakly-coupled wireless power transfer," *IEEE Trans. Power Electron.*, vol. 32, no. 9, pp. 7130–7139, Sep. 2017.

[6] Y. Li, J. Hu, F. Chen, Z. Li, Z. He, and R. Mai, "Dual-phase-shift control scheme with current-stress and efficiency optimization for wireless power transfer systems," *IEEE Trans. Circuits Syst. I, Reg. Papers*, vol. 65, no. 9, pp. 3110–3121, Sep. 2018.

[7] H. Li, J. Fang, S. Chen, K. Wang, and Y. Tang, "Pulse density modulation for maximum efficiency point tracking of wireless power transfer systems," *IEEE Trans. Power Electron.*, vol. 33, no. 6, pp. 5492–5501, Jun. 2018.

[8] F. Liu, Y. Yang, D. Jiang, X. Ruan, and X. Chen, "Modeling and optimization of magnetically coupled resonant wireless power transfer system with varying spatial scales," *IEEE Trans. Power Electron.*, vol. 32, no. 4, pp. 3240–3250, Apr. 2017.

[9] Z. Zhang, H. Pang, and J. Wang, "Multiple objective-based optimal energy distribution for wireless power transfer," *IEEE Trans. Magn.*, vol. 54, no. 11, pp. 1–5, Nov. 2018.

[10] P. Tan, T. Peng, and S. Cao, "Modeling and implementation of switching control for multi-transmitter wireless power transfer," in *Proc. IEEE Energy Convers. Congr. Exp. (ECCE)*, Sep. 2018, pp. 1987–1991.

[11] W. Zhang, T. Zhang, Q. Guo, L. Shao, N. Zhang, X. Jin, and J. Yang, "High-efficiency wireless power transfer system for 3D, unstationary free-positioning and multi-object charging," *IET Electr. Power Appl.*, vol. 12, no. 5, pp. 658–665, May 2018.

[12] P. K. S. Jayathurathnage, A. Alphones, D. M. Vilathgamuwa, and A. Ong, "Optimum transmitter current distribution for dynamic wireless power transfer with segmented array," *IEEE Trans. Microw. Theory Techn.*, vol. 66, no. 1, pp. 346–356, Jan. 2018.

[13] T. Arakawa, S. Goguri, J. V. Krogmeier, A. Kruger, D. J. Love, R. Mudumbai, and M. A. Swabey, "Optimizing wireless power transfer from multiple transmit coils," *IEEE Access*, vol. 6, pp. 23828–23838, 2018.

[14] S. Zhou and C. C. Mi, "Multi-paralleled LCC reactive power compensation networks and their tuning method for electric vehicle dynamic wireless charging," *IEEE Trans. Ind. Electron.*, vol. 63, no. 10, pp. 6546–6556, Oct. 2016.

[15] Y. Li, R. Mai, L. Lu, T. Lin, Y. Liu, and Z. He, "Analysis and transmitter currents decomposition based control for multiple overlapped transmitters based WPT systems considering cross couplings," *IEEE Trans. Power Electron.*, vol. 33, no. 2, pp. 1829–1842, Feb. 2018.

[16] H. Hao, G. A. Covic, and J. T. Boys, "A parallel topology for inductive power transfer power supplies," *IEEE Trans. Power Electron.*, vol. 29, no. 3, pp. 1140–1151, Mar. 2014.

[17] S. Moon and G.-W. Moon, "Wireless power transfer system with an asymmetric 4-coil resonator for electric vehicle battery chargers," *IEEE Trans. Power Electron.*, vol. 31, no. 10, pp. 6844–6854, Oct. 2016.

[18] Z. Liu, Z. Chen, Y. Guo, and Y. Yu, "A novel multi-coil magnetically-coupled resonance array for wireless power transfer system," in *Proc. IEEE Wireless Power Transf. Conf. (WPTC)*, May 2016, pp. 1–3.

[19] F. Lu, H. Zhang, H. Hofmann, W. Su, and C. C. Mi, "A dual-coupled LCC-compensated IPT system with a compact magnetic coupler," *IEEE Trans. Power Electron.*, vol. 33, no. 7, pp. 6391–6402, Jul. 2018.

[20] P. Jayathurathnage, D. M. Vilathgamuwa, S. D. Gregory, J. F. Fraser, and N. T. Tran, "Effects of adjacent transmitter current for multi-transmitter wireless power transfer," in *Proc. IEEE Southern Power Electron. Conf. (SPEC)*, Dec. 2017, pp. 1–4.

[21] X. Dai, X. Li, Y. Li, and A. P. Hu, "Impedance-matching range extension method for maximum power transfer tracking in IPT system," *IEEE Trans. Power Electron.*, vol. 33, no. 5, pp. 4419–4428, May 2018.

[22] X. Dai, J.-C. Jiang, and J.-Q. Wu, "Charging area determining and power enhancement method for multiexcitation unit configuration of wirelessly dynamic charging EV system," *IEEE Trans. Ind. Electron.*, vol. 66, no. 5, pp. 4086–4096, May 2019.

[23] Y.-G. Su, L. Chen, X.-Y. Wu, A. P. Hu, C.-S. Tang, and X. Dai, "Load and mutual inductance identification from the primary side of inductive power transfer system with parallel-tuned secondary power pickup," *IEEE Trans. Power Electron.*, vol. 33, no. 11, pp. 9952–9962, Nov. 2018.

[24] F. Liu, Z. Zhao, Y. Zhang, K. Chen, F. He, and L. Yuan, "A selection method of mutual inductance identification models based on sensitivity analysis for wireless electric vehicles charging," in *Proc. IEEE Energy Convers. Congr. Exposit. (ECCE)*, Sep. 2016, pp. 1–6.

[25] Y.-G. Su, H.-Y. Zhang, Z.-H. Wang, A. P. Hu, L. Chen, and Y. Sun, "Steady-state load identification method of inductive power transfer system based on switching capacitors," *IEEE Trans. Power Electron.*, vol. 30, no. 11, pp. 6349–6355, Nov. 2015.

[26] D. Kobayashi, T. Imura, and Y. Hori, "Real-time coupling coefficient estimation and maximum efficiency control on dynamic wireless power transfer for electric vehicles," in *Proc. IEEE PELS Workshop Emerg. Technol., Wireless Power (WoW)*, Jun. 2015, pp. 1–6.

XIN DAI (Member, IEEE) received the B.S. degree in industrial automation from Yuzhou University, Chongqing, China, in 2000, and the Ph.D. degree in control theory and control engineering from the School of Automation, Chongqing University, Chongqing, in 2006. In 2012, he was a Visiting Scholar with The University of Auckland, New Zealand. He is currently working as a Professor with the School of Automation, Chongqing University. His current research interests include inductive power transfer technology and nonlinear dynamic behavior analysis of power electronics.

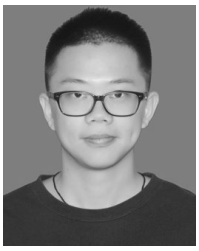

JINCHENG JIANG received the B.S. degree from the College of Optoelectronic Engineering, Chongqing University of Posts and Telecommunications, Chongqing, China, in 2015. He is currently pursuing the Ph.D. degree in control theory and control engineering with Chongqing University. His current research interests include the dynamic wireless charging systems and multi-excitation units wireless power transfer systems.

ZHOU XU received the M.S. degree from the College of Automation, Chongqing University, Chongqing, China, in 2018. His current research interests include the dynamic wireless charging systems and high frequency wireless power transfer systems.

YANLING LI received the Ph.D. degree from the School of Automation, Chongqing University, Chongqing, China, in 2017. She is currently working with the School of Electrical Engineering and Electronics Information, Xihua University, Chengdu, China. Her current research interests include wireless power transfer and advanced control technology in power electronics.